Japanese Journal of Applied Physics **50** (2011) 04DE07 **REGULAR PAPER**
DOI: 10.1143/JJAP.50.04DE07

A High-Linearity Low-Noise Amplifier with Variable Bandwidth for Neural Recoding Systems

Takeshi Yoshida, Katsuya Sueishi, Atsushi Iwata[1], Kojiro Matsushita[2], Masayuki Hirata[2], and Takafumi Suzuki[3]

Graduate School of Advanced Sciences of Matter, Hiroshima University, Higashihiroshima, Hiroshima 739-8530, Japan
[1]*A-R-Tech Corporation, Higashihiroshima, Hiroshima 739-0046, Japan*
[2]*Department of Neurosurgery, Osaka University Medical School, Suita, Osaka 565-0871, Japan*
[3]*Graduate School of Information Science and Technology, University of Tokyo, Bunkyo, Tokyo 113-8656, Japan*

Received September 21, 2010; revised November 11, 2010; accepted November 12, 2010; published online April 20, 2011

This paper describes a low-noise amplifier with multiple adjustable parameters for neural recording applications. An adjustable pseudo-resistor implemented by cascade metal–oxide–silicon field-effect transistors (MOSFETs) is proposed to achieve low-signal distortion and wide variable bandwidth range. The amplifier has been implemented in 0.18 μm standard complementary metal–oxide–semiconductor (CMOS) process and occupies 0.09 mm^2 on chip. The amplifier achieved a selectable voltage gain of 28 and 40 dB, variable bandwidth from 0.04 to 2.6 Hz, total harmonic distortion (THD) of 0.2% with 200 mV output swing, input referred noise of 2.5 μVrms over 0.1–100 Hz and 18.7 μW power consumption at a supply voltage of 1.8 V.

1. Introduction

Recently, a brain machine interface (BMI)/brain computer interface (BCI) has been researched in order to restore communication function for the severely disabled people due to amyotrophic lateral sclerosis, spinal injury, brain stroke, etc. Especially, electrocorticograms (ECoG) is attracting attention as a key signal to realize these systems.[1)] The ECoG has a signal bandwidth of 0.1 to 100 Hz, and signal amplitude of a few μV to 1 mV. Thus the low-noise amplifier for the ECoG detection should have an input referred noise of a few μV to detect accurately the signal with low frequency and small amplitude. Moreover, the low-noise amplifier requires a control of the signal bandwidth and a wide dynamic range because the ECoG detection and unwanted noise such as induced noise of AC power supply are input simultaneously.[2)] In this paper, a low-noise amplifier for the ECoG detection is proposed. The proposed amplifier was implemented in 0.18 μm standard complementary metal–oxide–semiconductor (CMOS) process and it achieved high linearity and wide variable range of signal bandwidth by using a resistor of the subthreshold-biased cascade metal–oxide–silicon field-effect transistors (MOSFETs) with a few TΩ.

2. Conventional Variable Bandwidth Low-Noise Amplifier for Neural Recording

Figure 1(a) shows a conventional variable bandwidth low-noise amplifier for neural recording system.[3–5)] The low-noise amplifier consists of operational transimpedance amplifier (OTA), AC coupled capacitors C_1, feedback capacitors C_2 and tunable pseudo-resistor as feedback resistor. The midband voltage gain is set by C_1/C_2, and the low-pass corner frequency is adjusted by the bandwidth of the OTA. The high-pass corner frequency is controlled by the tunable pseudo-resistors shown in Fig. 1(b). The tunable pseudo-resistors, which employ two identical pMOS transistors in symmetrical connections, avoid the large change of resistance value across the large output voltage swing. During the output voltage is higher than the common-mode voltage, the gate of M_1 and pseudo-resistor source node V_s are charged up, while the gate of M_2 and pseudo-resistor drain node V_d remain virtually constant. During this period, M_1 and M_2 are off-state and on-state respectively, therefore the voltage swing is applied to the virtually shunt M_1.

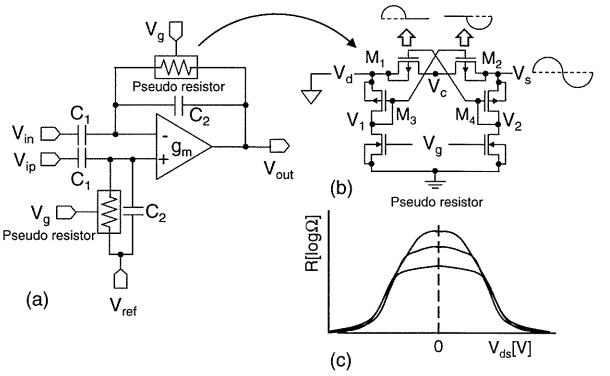

Fig. 1. (a) Conventional low-noise amplifier. (b) Schematic of pseudo resistor. (c) Resistance of the pseudo resistor.

Conversely, during the output voltage is lower than the common-mode voltage, the gate voltage of M_1 is pulled down below the common-mode voltage and move to turn on M_1, thereby the voltage swing is applied to the virtually shunt M_2. Accordingly, each pMOS transistor works as an active pseudo-resistor for each voltage range. The gate to source voltages of M_1 and M_2 are $(V_d - V_2)$ and $(V_s - V_1)$, respectively, each gate to source voltage of the shunt transistor is independent of V_d and V_s because of diode connected bias circuits. Thus the resistance of pseudo-resistor is not affected by the change of V_s. This technique yields a wide output voltage range and a few degradation of linearity but requires additional biasing circuitry [Figs. 1(b) and 1(c)].

A MOS-bipolar pseudo-resistor and a subthreshold-biased MOSFET as a feedback resistor with a high resistance are also used for biosignal amplifier.[6–10)] However, the MOS-bipolar pseudo-resistor is not able to adjust a resistance value, and it is possible to use the subthreshold-biased MOSFET with a high resistance while the gate-to-source voltage V_{gs} and the drain-to-source voltage V_{ds} of the MOSFET are small. When the output voltage swing of the biosignal amplifier will be large, a resistance value of the feedback resistor implemented by the MOSFET changes greatly and then it causes the deterioration of linearity. In case of adjusting low roll-off frequency of the amplifier using the gate voltage V_g, the linearity of the amplifier is worse. Thus it is necessary to suppress the degradation of linearity.

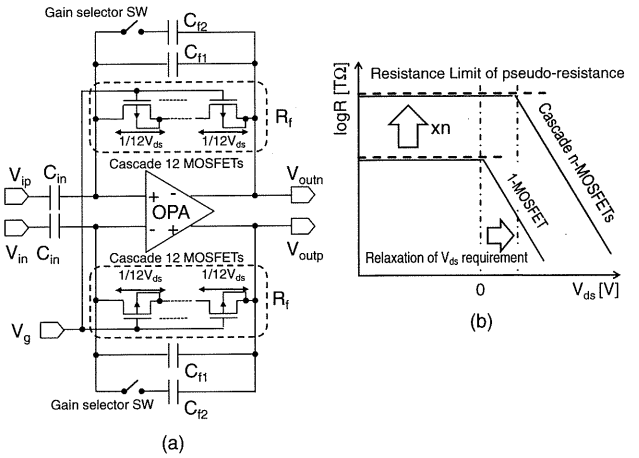

Fig. 2. (a) Schematic of proposed low-noise amplifier. (b) Conceptual diagram of the resistance characteristics using the cascade MOSFETs.

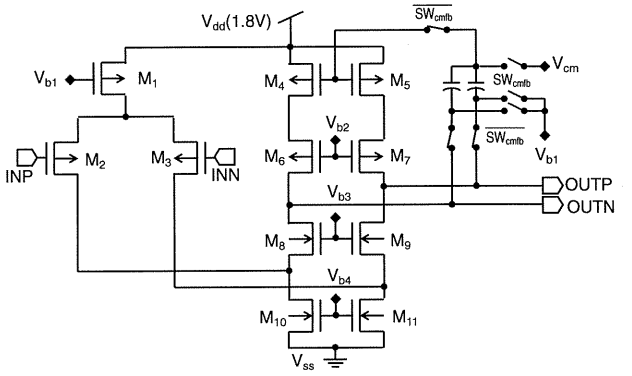

Fig. 3. Schematic of fully-differential opamp.

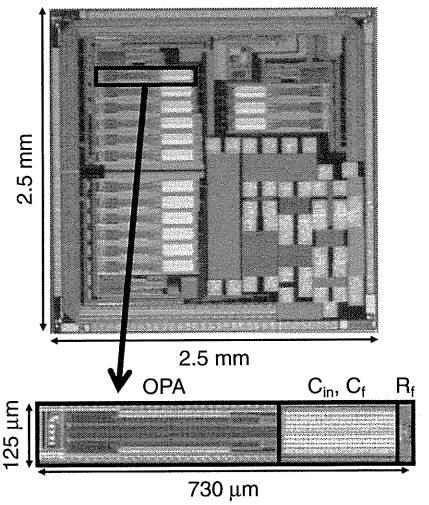

Fig. 4. (Color online) Chip micrograph of the proposed amplifier.

3. Proposed Low-Noise Amplifier

The schematic of a prototype low-noise amplifier is shown in Fig. 2(a). The low-noise amplifier consists of a fully-differential opamp, AC coupled capacitors C_{in}, feedback capacitors C_{f1} and C_{f2}, gain selector switches and feedback resistors R_f implemented by cascade MOSFETs, thus the low-noise amplifier realize high input impedance and a high-pass filter characteristic. A roll-off frequency of the high-pass filter is determined by both the R_f and the C_f, the roll-off frequency is given by $1/(2\pi R_f C_f)$. In case of a 0.18-µm CMOS technology, a capacitance value of the C_f, which is limited by parasitic components and characteristic deviation, is 50 fF. To achieve less than 0.01 Hz of low roll-off frequency, the resistance of R_f needs more than 318 TΩ. To solve the problem, we propose a tunable pseudo-resistor implemented by cascade MOSFETs operated in subthreshold region, as shown in Fig. 2(a). The proposed pseudo-resistor which is based on a MOS-bipolar pseudo-resistor[6] employs the V_g terminal for tuning the resistance value. A cascade MOSFETs structure can increase the resistance value in proportion to the number of connected MOSFET and moderates a change of a drain to source voltage V_{ds} of a MOSFET due to a resistance voltage divider. In this prototype, the pseudo-resistor has 12 MOSFETs, thereby the resistance of pseudo-resistor increases 12 times larger than the resistance of a MOSFET, and then the V_{ds} change of each MOSFET is reduced to 1/12. The conceptual diagram of the resistance characteristics using the cascade MOSFETs is shown in Fig. 2(b). The cascade MOSFETs improve the resistance limit and the output voltage range of the low-noise amplifier in proportion to the number of connected MOSFET. In addition, a wide variable range of bandwidth is accomplished with adjusting the V_g of MOSFET. In order to improve a low roll-off frequency of high-pass filter in the low-noise amplifier, at least 10 MOSFETs are needed for the pseudo-resistor.

Figure 3 shows the schematic of the fully-differential opamp in the low-noise amplifier. To achieve a high voltage gain and wide output swing, folded-cascode opamp is used. A $1/f$ noise of the opamp is decreased by enlarging the area of M_2 and M_3 that is the major factor of $1/f$ noise; however a power consumption of the opamp is increased because of the enlarging MOSFET area. Consequently, there is a trade-off between $1/f$ noise and power consumption. The SW_{cmfb} are switches for a common-mode feedback, these are operated at 32 kHz. Simulations show that the opamp has a voltage gain of 86.9 dB, phase margin of 89°, unity gain bandwidth of 40 kHz, and current consumption of 10 µA.

4. Experimental Results

A chip micrograph of the proposed amplifier fabricated by a 0.18 µm CMOS technology is shown in Fig. 4. It occupies 0.09 mm^2 of the chip area and dissipates 10.4 µA at a supply voltage of 1.8 V. The measured voltage gain of the amplifier is shown in Fig. 5. The midband voltage gain can be adjusted to 28 and 40 dB by the gain selector switch. The measured frequency response of the amplifier with variable low roll-off frequency is shown in Fig. 6. A 2 mV_{pp} sine wave is used at the input. The proposed amplifier achieved a variable bandwidth from 0.04 to 30 Hz by adjusting the gate voltage of cascade MOSFETs V_g from 0.75 to 1 V. The measured input referred noise of the amplifier with the maximum bandwidth is shown in Fig. 7. The rms value of the input referred noise is 2.5 µV integrated from 0.1 to 100 Hz. The large gate area of the input MOSFETs results in

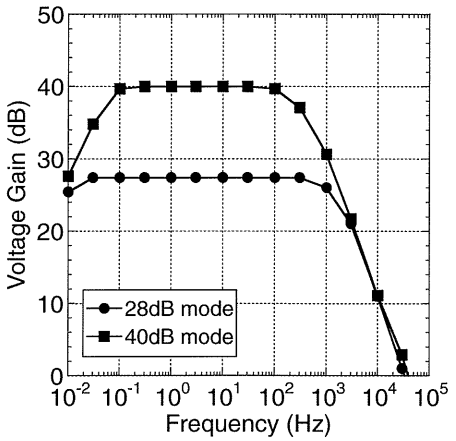

Fig. 5. Measured voltage gain of the proposed amplifier.

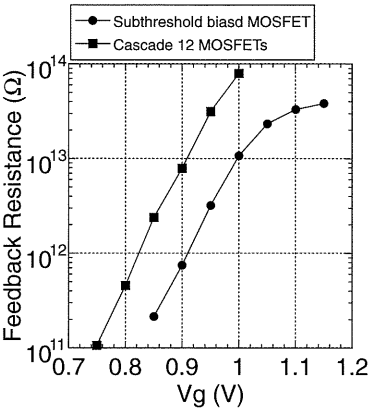

Fig. 8. Measured resistance of feedback resistor implemented by the cascade connected 12 MOSFETs.

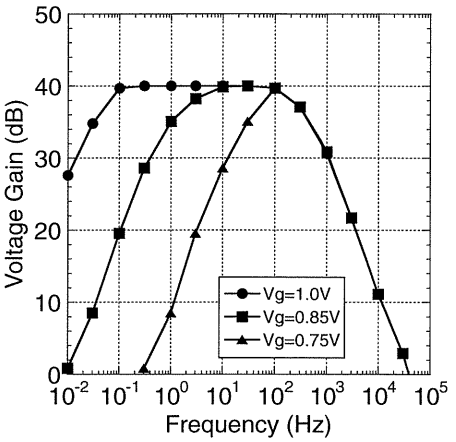

Fig. 6. Measured frequency response of the proposed amplifier with variable low roll-off frequency.

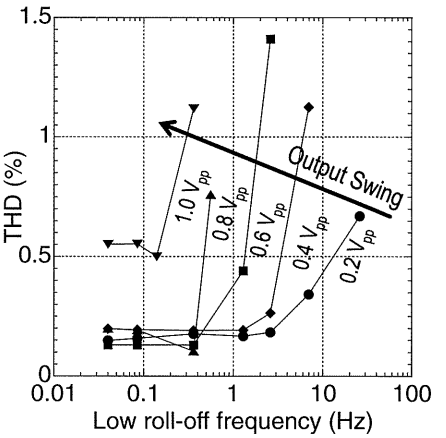

Fig. 9. Measured total harmonic distortion of the proposed amplifier against the output amplitude.

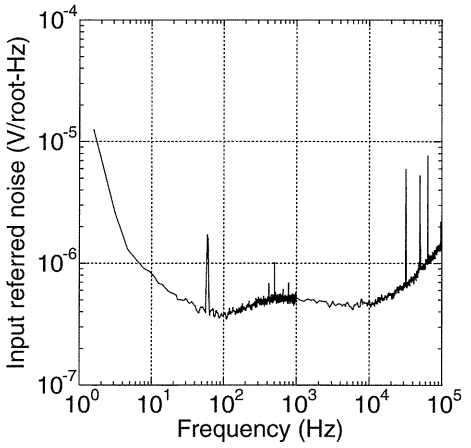

Fig. 7. Measured input referred noise of the proposed amplifier.

a low corner frequency of $1/f$ noise. The observed spectra at 60 Hz and 32 kHz are caused by a power supply noise and a clock signal for common-mode feedback, respectively.

Figure 8 shows the resistance value of the feedback resistor implemented by the cascade connected 12 MOSFETs that are calculated by the measured roll-off frequency. By comparison, the resistance value of a subthreshold biased MOSFET is also shown in Fig. 8. The resistance of the subthreshold biased MOSFET is becoming saturated at 30 TΩ, however the cascade connected 12 MOSFETs achieved more than the resistance of 80 TΩ.

The measured total harmonic distortion (THD) against the low roll-off frequency of the amplifier is plotted in Fig. 9. Sine wave inputs with different amplitude levels of 2, 4, 6, 8, and 10 mV are applied to the amplifier. In the case of 2 mV input (0.2 V_{pp} output swing), the THD is less than 0.2% from the roll-off frequency of 0.04 Hz to that of 2.6 Hz. Thus the proposed amplifier with the cascade connected 12 MOSFETs can control low roll-off frequency range of triple-digits with maintenance of a high linearity. The performance comparison with other low-noise amplifier for neural recordings is summarized in Table I.

5. Conclusions

Low-noise amplifier with high linearity and wide variable range of bandwidth is proposed. When defining 0.2 V_{pp} output swing, the proposed amplifiers with a feedback resistor of cascade connected 12 MOSFETs operated in the subthreshold achieved a variable low roll-off frequency of

Table I. Performance comparison with the reference low-noise amplifiers and this study.

Parameter	Ref. 3	Ref. 4	Ref. 6	This work
Supply voltage (V)	1.8	1	±2.5	1.8
Technology	0.8 μm CMOS	0.35 μm CMOS	1.5 μm CMOS	0.18 μm CMOS
Current (μA)	1.2	0.337	0.18	10.4
Midband gain (dB)	41/50.5	45.6/49/53.5/60	39.8	28/40
High-pass f-3dB (Hz)	0.05/0.4/2.5	0.0045–3.6	0.014	0.04–2.6
Low-pass f-3dB (Hz)	180	31–292	30	100
Input referred noise (μV)	0.93 (0.5–100 Hz)	2.5 (0.05–460 Hz)	1.6 (0.5–30 Hz)	2.5 (0.1–100 Hz)
CMRR (dB)	105	71.2	86	76.9
PSRR (dB)	—	84	80	86
THD (%)	—	<0.6	<1.0	<0.2
Area (mm^2)	1.4	0.64	0.22	0.09

0.04–2.6 Hz and less than the THD of 0.2%. The input referred noise is 2.5 μV_{rms} over 0.1–100 Hz. The amplifier consumes a chip area of 0.09 mm^2 and a power consumption of 18.7 μW at a supply voltage of 1.8 V.

Acknowledgements

This work was supported in part by the Strategic Research Program for Brain Sciences, Grants-in-Aid for Scientific Research (20300199) from Japan Society for the Promotion of Science (JSPS). The VLSI chip in this study has been fabricated in the chip fabrication program of VLSI Design and Education Center (VDEC), the University of Tokyo in collaboration with Rohm Corporation and Toppan Printing Corporation.

1) A. Schlogl, F. Lee, H. Bischof, and G. Pfurtscheller: J. Neural Eng. **2** (2005) L14.
2) T. Yoshida, Y. Masui, R. Eki, A. Iwata, M. Yoshida, and K. Uematsu: IEICE Trans. Electron. **E93-C** (2010) 849.
3) T. Denison, K. Consoer, A. Kelly, A. Hachenburg, and W. Santa: ISSCC Dig. Tech. Pap., 2007, p. 162.
4) X. Y. Xu, X. D. Zou, L. B. Yao, and Y. Lian: 2008 Symp. VLSI Circuits Dig. Tech. Pap., 2008, p. 78.
5) X. Zou, X. Xu, L. Yao, and Y. Lian: IEEE J. Solid-State Circuits **44** (2009) 1067.
6) R. R. Harrison and C. Charles: IEEE J. Solid-State Circuits **38** (2003) 958.
7) R. H. Olsson III, D. L. Buhl, A. M. Sirota, G. Buzsaki, and K. D. Wise: IEEE Trans. Biomed. Eng. **52** (2005) 1303.
8) T. Horiuchi, T. Swindell, D. Sander, and P. Abshire: Proc. ISCAS, 2004, p. 29.
9) W. Wattanapanitch, M. Fee, and R. Sarpeshkar: IEEE Trans. Biomed. Circuits Syst. **1** (2007) 136.
10) M. Yin and M. Ghovanloo: Proc. ISCAS, 2007, p. 321.

PAIN® 152 (2011) 860–865

PAIN®

www.elsevier.com/locate/pain

Deep brain stimulation of the subthalamic nucleus improves temperature sensation in patients with Parkinson's disease

Tomoyuki Maruo [a], Youichi Saitoh [a,b,*], Koichi Hosomi [a,b], Haruhiko Kishima [a], Toshio Shimokawa [c], Masayuki Hirata [a], Tetsu Goto [a], Shayne Morris [a], Yu Harada [a], Takufumi Yanagisawa [a], Mohamed M. Aly [a], Toshiki Yoshimine [a]

[a] *Department of Neurosurgery, Osaka University Graduate School of Medicine, Osaka, Japan*
[b] *Department of Neuromodulation and Neurosurgery, Center for Advanced Science and Innovation, Osaka University, Osaka, Japan*
[c] *Department of Ecosocial System Engineering, Graduate School of Medicine and Engineering, University of Yamanashi, Yamanashi, Japan*

Sponsorships or competing interests that may be relevant to content are disclosed at the end of this article.

ARTICLE INFO

Article history:
Received 4 August 2010
Received in revised form 23 November 2010
Accepted 21 December 2010

Keywords:
Parkinson's disease
Deep brain stimulation
Quantitative sensory testing
Cold and warm sense threshold
Cold and heat pain threshold

ABSTRACT

Patients with Parkinson's disease (PD) reportedly show deficits in sensory processing in addition to motor symptoms. However, little is known about the effects of bilateral deep brain stimulation of the subthalamic nucleus (STN-DBS) on temperature sensation as measured by quantitative sensory testing (QST). This study was designed to quantitatively evaluate the effects of STN-DBS on temperature sensation and pain in PD patients. We conducted a QST study comparing the effects of STN-DBS on cold sense thresholds (CSTs) and warm sense thresholds (WSTs) as well as on cold-induced and heat-induced pain thresholds (CPT and HPT) in 17 PD patients and 14 healthy control subjects. The CSTs and WSTs of patients were significantly smaller during the DBS-on mode when compared with the DBS-off mode ($P < .001$), whereas the CSTs and WSTs of patients in the DBS-off mode were significantly greater than those of healthy control subjects ($P < .02$). The CPTs and HPTs in PD patients were significantly larger on the more affected side than on the less affected side ($P < .02$). Because elevations in thermal sense and pain thresholds of QST are reportedly almost compatible with decreases in sensation, our findings confirm that temperature sensations may be disturbed in PD patients when compared with healthy persons and that STN-DBS can be used to improve temperature sensation in these patients. The mechanisms underlying our findings are not well understood, but improvement in temperature sensation appears to be a sign of modulation of disease-related brain network abnormalities.

1. Introduction

Deep brain stimulation of the subthalamic nucleus (STN-DBS) is effective in treating patients with advanced-stage Parkinson's disease (PD) [10,11]. It is particularly effective for improving motor functional impairment, a deficit that originates from altered peripheral feedback or abnormal central processing [2,9]. In addition to motor symptoms, sensory disturbances are part of the clinical picture of PD. PD patients frequently experience pain, numbness, and decreased proprioception, all of which are thought to result from deficient gating of sensory information due to basal ganglia dysfunction [8]. These sensory disturbances could be factors contributing to motor deficits [7,16]. It is important to recognize sensory disturbances because they can lead to even more serious complications and diminish quality of life.

Little is known about the effects of STN-DBS on sensory symptoms and the mechanisms by which STN-DBS alleviates sensory symptoms in PD. The effects of treating PD patients are usually assessed using the Unified Parkinson's Disease Rating Scale (UPDRS). Although the UPDRS allows appropriate evaluation of motor symptoms and functional disability, it is not suitable for evaluating sensory symptoms. Recently, sensory dysfunction has been measured for pain symptoms in PD patients using quantitative measurements [3], by electrophysiological methods, and by recording laser-evoked potentials [20]. In particular, quantitative measurement has increasingly been used for assessment of sensory thresholds in epidemiologic, clinical, and research studies [4]. Differences in thermal quantitative sensory testing (QST) are also reportedly compatible with elevations in temperature sense thresholds and pain thresholds [6]. We were therefore interested in quantitatively evaluating temperature sensations as well as pain in PD patients with the use

* Corresponding author at: Department of Neurosurgery, Osaka University Graduate School of Medicine, 2-2 Yamadaoka, Suita, Osaka 565-0871, Japan. Tel.: +81 6 6879 3652; fax: +81 6 6879 3659.
E-mail address: saitoh@nsurg.med.osaka-u.ac.jp (Y. Saitoh).

0304-3959/$36.00
doi:10.1016/j.pain.2010.12.038

of thermal QST studies. The aim of our study was to quantitatively evaluate the effects of STN-DBS on temperature sensations and pain, in hopes of improving the diagnosis and treatment of PD patients. Thus, we conducted a QST study to assess the effects of STN-DBS on both temperature sensation and pain in PD patients compared with healthy control subjects.

2. Methods

2.1. Subjects

Our study involved 2 groups of subjects: 17 patients with idiopathic PD diagnosed based on the diagnostic criteria of the UK Parkinson's Disease Society Brain Bank (6 men, 11 women; mean age: 65.7 ± 3.8 years, range: 55 to 73 years) and 14 healthy control subjects (7 men, 7 women; mean age: 54.8 ± 14.0 years, range: 28 to 74 years). The latter were selected from healthy volunteers free of central nervous system disease. All patients who underwent bilateral STN-DBS at Osaka University Hospital during the period from 2001 through 2009 were included in this study. For STN-DBS, standard surgery inclusion/exclusion criteria were applied to all cases. At the time of enrollment in the study, most patients had normal intelligence as defined by a Mini-Mental State Examination score $\geqslant 25$ and correct language comprehension. UPDRS motor scores had been obtained for all patients during DBS-on and DBS-off states. Cold sense thresholds (CSTs), warm sense thresholds (WSTs), cold pain thresholds (CPTs), and heat pain thresholds (HPTs) were determined on the palms of the subjects' hands. Both the more affected and the less affected sides were assessed in PD patients. Thus, the side more affected by the disease was the side with the higher UPDRS score in the PD patients. In addition to age and sex, the following clinical variables were assessed for each patient: disease duration, Hoehn and Yahr disease stage, UPDRS motor scores during DBS-on and DBS-off states, and the DBS amplitude at study enrollment. The Ethics Committee of Osaka University Hospital approved this study, and informed consent was obtained from all participants (approval number: 09213).

2.2. QST protocol

QST was performed with a thermal sensory analyzer (PATHWAY Pain and Sensory Evaluation System; Medoc Ltd, Ramat Yishai, Israel). The computer driven PATHWAY system contains a metal contact plate (30 × 30 mm) that can be cooled and heated by an external Peltier element and is used to assess sensory thresholds. Peltier devices can change temperature at a predictable rate and can be used to test CSTs, WSTs, CPTs, and HPTs.

CSTs, WSTs, CPTs, and HPTs were examined in all study subjects by 1 of 2 examiners (T.M. or K.H.) who followed a standardized procedure. The testing was performed in a quiet room kept at a constant temperature (21°C to 25°C), with each subject resting comfortably in a sitting position. The 9-cm^2 Peltier probe was placed on the palm of the hand on the tested side and fastened with an elastic Velcro strap. The baseline temperature of the probe was 32°C, and the temperature was set to change at a rate of 1°C/s until a minimum temperature of 0°C or a maximum temperature of 51°C was reached, or until the subject pressed a response button held in their opposite hand [14,18,24]. For safety reasons, a maximum temperature of 51°C and a minimum temperature of 0°C were chosen to prevent cutaneous burns. The method of limits was used to determine all thresholds [18]. To determine CSTs, WSTs, CPTs, and HPTs, the subjects were asked to press a response button held in the opposite hand to that being tested, when cold or warm sensations and cold or hot pain sensation were respectively first perceived, starting from a baseline temperature of 32°C [23,25]. The CST and WST thresholds were defined as the absolute value of the temperature change from the baseline of 32°C at which subjects indicated their first cold or warm sensations, respectively. The CPTs and HPTs were also defined as the absolute value of the temperature change from baseline at which subjects indicated the point where a respective cold or warm temperature became painful. For each of the 4 types of threshold, the test was repeated 4 times in a uniform manner. Threshold tests began with temperature sensory thresholds for cold then warm, followed by pain thresholds for cold then heat. QSTs were first performed on the right hand and then on the left hand. The mean value from the 4 tests was taken as the threshold value. For PD patients, each test was performed bilaterally in both the DBS-on and the DBS-off state, the latter being undertaken approximately 30 minutes after the stimulator was switched off (Fig. 1). For healthy control subjects, each test was performed twice with a 30-minute interval between tests to examine the effects of repetitive QST on normal subjects.

Threshold values are expressed in degrees Centigrade. The lower the temperature (below 32°C) to which a subject responded, the greater the CST or CPT; the higher the temperature (above 32°C) to which a subject responded, the greater the WST or HPT. After the maximum or minimum temperature was reached or the subject indicated a sensory threshold by pressing the response button, the temperature automatically returned to the baseline of 32°C. The temperature was set to return at a rate of 2°C/s for temperature sensation thresholds and 8°C/s for pain thresholds. To prevent possible modulation of thermal receptors, in the case of temperature threshold measurements, the metal contact plate remained at the baseline temperature for 5 seconds before temperatures increased or decreased. In the case of pain threshold measurements, this interval was 10 seconds [24]. Before the actual tests, all subjects participated in a short training session to make sure they understood the test procedure.

2.3. Statistical analysis

A descriptive statistical analysis was performed on all data. Median values were used for all variables to indicate thermal thresholds. A Dunnett multiple comparisons test was used to analyze differences in test results between the PD patients and the healthy control subjects. For the PD patient group, differences in temperature sense thresholds and pain thresholds between the DBS-off and DBS-on states and between the more affected and less affected sides were analyzed with a 2-factor repeated-measures analysis of variance (ANOVA). The 1-way repeated-measures ANOVA was used to test for correlations between clinical variables and QST scores. A value of $P < .05$ was considered statistically significant. SPSS for Windows 17.0 was used for all statistical analyses (SPSS Inc., Chicago, IL, USA)

3. Results

3.1. Clinical assessment

QST data were obtained for all 17 PD patients and all 14 control subjects. Clinical characteristics of the 17 PD patients are shown in detail in Table 1. The mean duration of PD at the time of testing was 15.5 ± 5.4 years. Hoehn and Yahr stages ranged from 2 to 3. The mean UPDRS motor score was 22.0 ± 7.8 during the DBS-on state and 36.3 ± 11.8 during the DBS-off state. All patients treated with STN-DBS, levodopa, and dopamine agonists showed marked improvement in UPDRS motor scores. There were no significant correlations between the sensory threshold values and patient characteristics (age, sex, Hoehn and Yahr stage, disease duration, UPDRS score, or DBS amplitude).

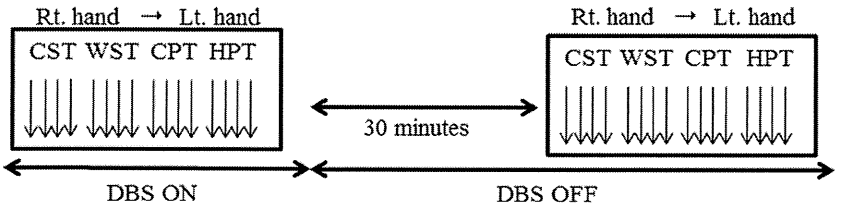

Fig. 1. Diagram of the QST protocol. For each type of threshold, the test was repeated 4 times, first on the right hand then on the left hand, and the mean value from the 4 tests was taken as the threshold value. For patients with PD, each test was performed both in the bilateral DBS-on state and DBS-off state (30 minutes after switching the stimulator off). CPT, cold pain threshold; CST, cold sense threshold; DBS-on, deep brain stimulation on; DBS-off, deep brain stimulation off; HPT, heat pain threshold; PD, Parkinson's disease; WST, warm sense threshold.

3.2. Differences in sensory thresholds between PD patients and control subjects

CSTs and WSTs of the PD patients and control subjects are shown in Fig. 2 and Table 2. CSTs were significantly greater in PD patients in the DBS-off state than in control subjects (27.5 ± 0.8°C [less affected side] vs 30.9 ± 0.2°C [control], $P = .010$; 25.6 ± 1.0°C [more affected side] vs 30.9 ± 0.2°C [control], $P < .001$). However, CSTs did not differ significantly between PD patients in the DBS-on mode and control subjects (29.7 ± 0.3°C [less affected side] vs 30.9 ± 0.2°C [control], NS; 29.0 ± 0.6°C [more affected side] vs 30.9 ± 0.2°C [control], NS). WSTs were significantly greater in PD patients in the DBS-off state than in control subjects (36.2 ± 0.6°C [less affected side] vs 33.9 ± 0.3°C [control], $P = .013$; 36.7 ± 0.8°C [more affected side] vs 33.9 ± 0.3°C [control], $P = .002$). However, WSTs did not differ significantly between PD patients in the DBS-on state and control subjects (34.5 ± 0.3°C [less affected side] vs 33.9 ± 0.3°C [control], NS; 34.5 ± 0.3°C [more affected side] vs 33.9 ± 0.3°C [control], NS). There were no significant differences in either CPTs or HPTs between PD patients (in both DBS-on and DBS-off states) and control subjects.

3.3. Differences in sensory thresholds between DBS-on and DBS-off modes

There were no significant differences in any of the thresholds of the healthy control subjects over the 2 sessions with a 30-minute interval in between (Table 3). In the patient group, there were significant differences in CSTs and WSTs between the DBS-on and DBS-off states. CSTs were significantly lower during the DBS-on state than during the DBS-off state (DBS-on 29.4°C vs DBS-off 26.6°C, $P < .001$), with a significant difference between the more affected and less affected sides (less affected side 27.3°C vs more affected side 28.6°C, $P = .020$) (Fig. 3, Table 3). WSTs were significantly lower during the DBS-on state than during the DBS-off state (DBS-on 34.5°C vs DBS-off 36.5°C, $P < .001$), with no significant difference between the more affected and less affected sides (less affected side 35.6°C vs more affected side 35.4°C). CPTs and HPTs did not differ significantly with respect to the DBS mode; however, CPTs ($P = .011$) and HPTs ($P = .016$) were significantly lower on the less affected side than on the more affected side.

4. Discussion

Our 2 main findings were that, firstly, significantly greater CSTs and WSTs were observed in PD patients when compared with healthy control subjects, indicating that temperature sensation is indeed impaired in PD patients. Secondly, in our patients, CSTs and WSTs were significantly reduced during the DBS-on state when compared with the DBS-off state, suggesting that STN-DBS improves temperature sensation impairments in PD patients. To our knowledge, this is the first study to quantitatively document the effects of STN-DBS on temperature sensation in PD patients.

Table 1
Patients with PD clinical characteristics.

Patient no.	Age (y)	Sex	Disease duration (y)	Duration since STN DBS implant (mo)	H&Y stage	Medication (LEDD mg/d)	UPDRS motor score		MMSE	DBS mode	DBS amplitude	
							DBS-on	DBS-off			Rt	Lt
1	62	F	10	42	2	100	25	30	28	Bipolar	2.6	2.8
2	60	F	11	22	2	300	20	26	30	Monopolar	2.5	2.5
3	55	M	15	30	2	150	5	21	30	Monopolar	3.5	3.5
4	73	F	28	64	3	900	31	40	25	Monopolar	3.0	3.2
5	73	F	21	24	2	300	35	58	25	Bipolar	3.7	3.8
6	71	M	8	20	2	400	15	25	27	Monopolar	2.0	2.1
7	70	F	19	7	3	450	10	25	30	Monopolar	3.5	3.5
8	63	F	18	78	2	500	10	29	28	Monopolar	2.4	2.4
9	73	M	6	18	3	300	5	9	27	Monopolar	2.4	1.7
10	58	M	9	24	2	150	10	25	28	Monopolar	2.2	2.2
11	70	F	8	6	2	150	15	20	29	Monopolar	2.4	2.2
12	63	F	14	70	2	500	21	53	26	Monopolar	2.3	2.3
13	71	F	14	18	2	200	12	38	28	Monopolar	2.2	1.8
14	68	M	8	12	2	500	16	67	28	Monopolar	2.3	3.6
15	73	M	18	87	3	600	33	45	21	Monopolar	3.0	3.1
16	60	F	22	3	2	500	15	32	28	Monopolar	1.3	1.5
17	62	F	14	5	2	400	25	30	28	Monopolar	2.1	2.2
Means ± SD	65.7 ± 3.8		15.5 ± 5.4	31.1 ± 21.8	2.4 ± 0.4	406 ± 195	22.0 ± 7.8	36.3 ± 11.8	27 ± 2		2.5 ± 0.5	2.6 ± 0.6

LEDD, levodopa-equivalent daily dose; PD, Parkinson's disease"; H&Y, modified Hoehn and Yahr scale score"; STN, subthalamic nucleus; L-dopa, levodopa; UPDRS, unified Parkinson's disease rating scale; DBS, deep brain stimulation; MMSE, mini-mental state examination.

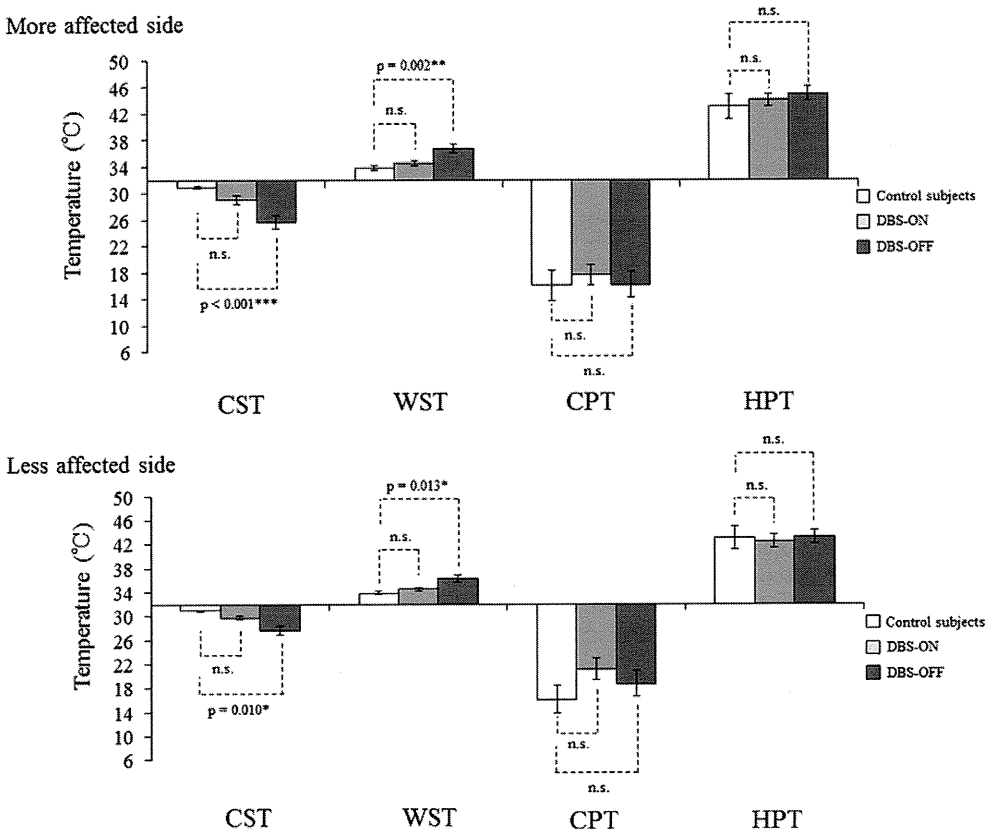

Fig. 2. Sensory thresholds in PD patients in the DBS-on state and DBS-off state compared with healthy control subjects. CSTs and WSTs were significantly greater in PD patients in the DBS-off state than in the healthy control subjects. Sensory threshold values are expressed in degrees Celsius. Mean values are shown (error bars represent SEM). A *P* value of <.05 was considered statistically significant (**P* < .05; ***P* < .01; ****P* < .001; NS, *P* > .05). CPT, cold pain threshold; CST, cold sense threshold; DBS-on, deep brain stimulation on; DBS-off, deep brain stimulation off; HPT, heat pain threshold; PD, Parkinson's disease; WST, warm sense threshold.

Sensory disturbances, which can either accompany or precede PD-associated motor disorders, are part of the clinical picture of PD and are most frequent in PD cases with motor complications [21]. It has been recommended that thermal QST for temperature sensation and pain are incorporated into routine neurological assessments [23]. QST of thermal modalities has been reported suitable for the screening and long-term evaluation of sensory function and useful for advancing somatosensory research [26]. In response, we hypothesized that QST for thermal thresholds may be useful for evaluating the sensory symptoms of PD. Patients with PD (in comparison to normal subjects) have been reported to show sensory impairment, with increased sensory thresholds for vibration [15] and increased 2-point discrimination thresholds in proprioception [17]. In a more recent study, PD patients showed sensory disturbances with decreased pain thresholds for cold and heat [3]. Thus, our CST and WST findings (Fig. 2) are consistent with previously reported studies demonstrating increased temperature sensory thresholds in PD patients [12].

The physiological mechanisms by which STN-DBS might improve temperature sensations in PD patients remains unclear; however, several hypotheses have been reported. Firstly, STN stimulation may lead indirectly to the activation of the somatosensory cortex and thereby lead to improved temperature sensation. In a previous FDG-PET study of bilateral STN-DBS, it was shown that during the DBS-on state, the regional cerebral metabolic rate of glucose consumption increased significantly in the midbrain, basal

Table 2
Sensory threshold in patients and control subjects.

	CSTs	WSTs	CPTs	HPTs	CSTs	WSTs	CPTs	HPTs
Control subjects	30.9 ± 0.2	33.9 ± 0.3	16.0 ± 2.3	43.0 ± 1.9				
		More affected side			Less affected side			
PD patients in DBS-on	29.0 ± 0.6	34.5 ± 0.3	17.7 ± 1.5	44.0 ± 0.9	29.7 ± 0.3	34.5 ± 0.3	21.1 ± 1.8	42.5 ± 1.1
PD patients in DBS-off	25.6 ± 1.0	36.7 ± 0.8	16.2 ± 2.0	45.0 ± 1.1	27.5 ± 0.8	36.2 ± 0.6	18.7 ± 2.1	43.2 ± 1.2
P value[a]	NS	NS	NS	NS	NS	NS	NS	NS
P value[b]	<.001***	.002**	NS	NS	.010*	.013*	NS	NS

P > .05 by Dunnett multiple comparisons test. CST, cold sense threshold; WST, warm sense threshold; CPT, cold pain threshold; HPT, heat pain threshold; PD, Parkinson's disease; DBS-on, deep brain stimulation on; DBS-off, deep brain stimulation off; NS, not significant.

[a] Comparison between PD patients in the DBS-on mode and healthy control subjects.

[b] Comparison between PD patients in the DBS-off mode and healthy control subjects.

* *P* < .05.

** *P* < .01.

*** *P* < .001.

Table 3
Sensory thresholds in patients with PD.

	CSTs	WSTs	CPTs	HPTs
Control subjects	30.9 ± 0.1	33.9 ± 0.1	16.0 ± 1.7	43.0 ± 1.1
Control subjects (after the interval of 30 minutes)	30.7 ± 0.1	34.0 ± 0.3	15.9 ± 2.2	42.8 ± 1.8
P value	NS	NS	NS	NS
DBS-on (PD patients)	29.4 ± 0.8	34.5 ± 0.7	19.4 ± 1.6	43.2 ± 1.0
DBS-off (PD patients)	26.6 ± 0.8	36.5 ± 0.7	17.4 ± 1.6	44.1 ± 1.0
P value[a]	<.001***	<.001***	NS	NS
More affected side (PD patients)	27.3 ± 0.8	35.6 ± 0.7	16.9 ± 1.6	44.5 ± 1.0
Less affected side (PD patients)	28.6 ± 0.8	35.4 ± 0.7	19.9 ± 1.6	42.8 ± 1.0
P value[b]	.020*	NS	.011**	.016**

NS = $P > .05$. CST, cold sense threshold; WST, warm sense threshold; CPT, cold pain threshold; HPT, heat pain threshold; PD, Parkinson's disease; DBS-on, deep brain stimulation on; DBS-off, deep brain stimulation off; NS, not significant.
[a] Comparison between PD in the DBS-on mode and PD in the DBS-off mode.
[b] Comparison between the less affected side and the more affected side in PD patients.
* $P < .05$.
** $P < .01$.
*** $P < .001$.

ganglia area, frontal cortex, temporal cortex, and parietal cortex [5,22]. It has been determined that the posterior parietal region received afferents from prefrontal regions, the sensory cortex, and multiple thalamic relay nuclei [19]. Thus, STN-DBS may activate not only the frontal but also the parietal cortex, and a contribution of STN to sensory function, as well as to its roles in associative, limbic, and basal ganglia circuits, has been confirmed [5]. This metabolic change may result in an altered temperature sensation that is associated with parietal and basal ganglia circuits. Secondly, STN-DBS might normalize brain network abnormalities related to temperature sensation and pain perception. PD reportedly involves a generalized dysfunction of the entire neuronal network, probably resulting from impaired basal ganglia function, although the precise mechanism is not well understood [17].

In this study, we have used the method of limits for performing QST. It has been reported that sensory thresholds are dependent on a subject's reaction time in the method of limits [18]. Thus we may need to take into account the result of biased reaction times as a result of possible motor impairment, especially when undertaking QST on the less affected side of PD patients, because this may introduce a delayed response when they click the response button with their opposite and more affected side hand. If this was to have a significant impact on the final results, we would expect lower thresholds for CSTs and WSTs of the less affected hand. Despite this

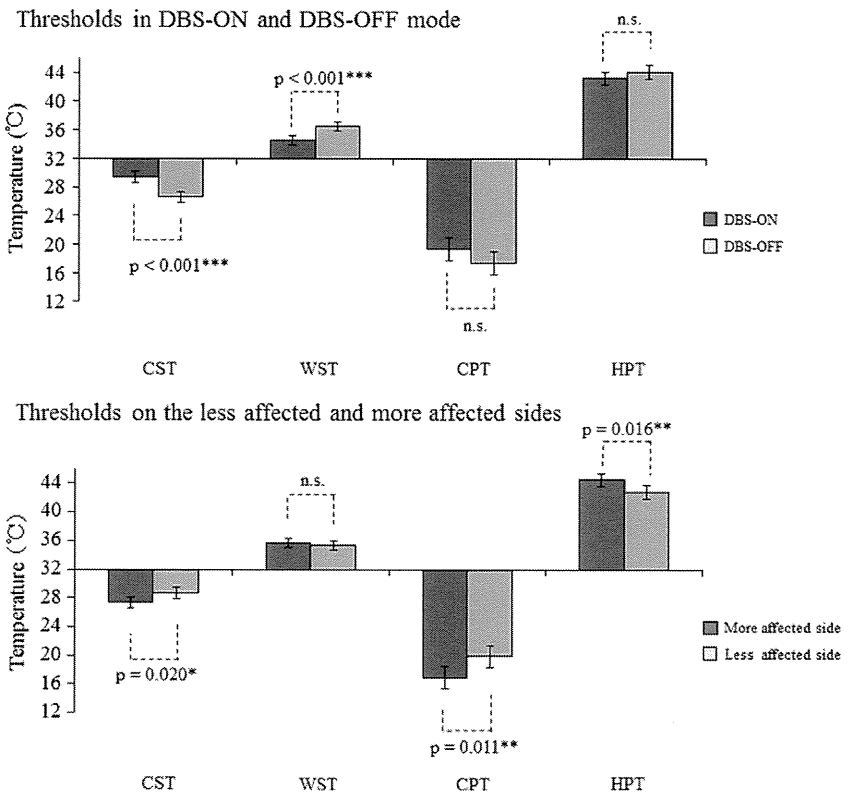

Fig. 3. Differences in sensory thresholds in patients with PD. CSTs and WSTs were significantly lower during the DBS-on state compared with the DBS-off state. CPTs and HPTs did not differ significantly between the DBS-on and DBS-off states. CPTs and HPTs were significantly lower on the less affected side than on the more affected side. A 2-factor repeated measures analysis of variance (ANOVA) was used to analyze differences. Error bars represent SEM. A *P* value of <.05 was considered statistically significant (*$P < .05$; **$P < .01$; ***$P < .001$; NS, $P > .05$). CPT, cold pain threshold; CST, cold sense threshold; DBS-on, deep brain stimulation on; DBS-off, deep brain stimulation off; HPT, heat pain threshold; PD, Parkinson's disease; WST, warm sense threshold.

possible bias, this was not the case. As was stated previously, the more affected hand was found to have lower thresholds for CSTs and WSTs. This would indicate that motor performance probably has little effect on the significance of the QST results in our study.

QST can be adversely affected by consecutive repeated tests. CSTs, WSTs, CPTs, and HPTs reportedly changed significantly with repeated testing [13]. Thus, researchers must be cautious when assessing the importance of changes in thermal sense thresholds. With this in mind, we performed a control experiment involving repeated QSTs with a 30-minute interval in between in 14 healthy control subjects. As a result, we found no significant differences between these 2 sessions separated by the interval of 30 minutes (Table 3). This result indicates that the sensory thresholds, CSTs and WSTs in particular, are probably not affected by repetitive QSTs separated by an interval of 30 minutes.

Only a few studies have addressed the effects of levodopa and dopamine agonists on sensory disorders in PD patients. Levodopa significantly reduced pain-induced activation in the posterior insula and anterior cingulate cortex in PD patients [1]. Our study did not include a baseline condition in which patients were completely free of antiparkinsonian medication. Indeed, the effect of levodopa on temperature sense thresholds may have influenced our results. However, it was not ethically possible for us to withdraw these medications from participating patients. It should, however, be noted that we consider the effects of drugs on our final results in this study to be minimized because DBS-on and DBS-off state temperature sensory thresholds and pain thresholds were compared in the same patients with all QST measurements being conducted within 1 hour of each other.

Our findings provide new insights into the mechanisms by which DBS improves sensory impairments, that is, via modulation of the disease-related brain network abnormality. Our findings suggest that STN-DBS can be used to modulate sensory pathways and improve temperature sensations in PD patients. Studies involving larger groups of patients are needed to show whether our findings reflect a general principle underlying the effect of STN-DBS on sensory information processing.

Acknowledgements

This study was supported in part by the Grant-in-Aid for Scientific Research from the Japanese Ministry of Health, Labour and Welfare. There are no conflicts of interest.

References

[1] Brefel-Courbon C, Payoux P, Thalamas C, Ory F, Quelven I, Chollet F, Montastruc JL, Rascol O. Effect of levodopa on pain threshold in Parkinson's disease: a clinical and positron emission tomography study. Mov Disord 2005;20:1557–63.

[2] Deuschl G, Schade-Brittinger C, Krack P, Volkmann J, Schafer H, Botzel K, Daniels C, Deutschlander A, Dillmann U, Eisner W, Gruber D, Hamel W, Herzog J, Hilker R, Klebe S, Kloss M, Koy J, Krause M, Kupsch A, Lorenz D, Lorenzl S, Mehdorn HM, Moringlane JR, Oertel W, Pinsker MO, Reichmann H, Reuss A, Schneider GH, Schnitzler A, Steude U, Sturm V, Timmermann L, Tronnier V, Trottenberg T, Wojtecki L, Wolf E, Poewe W, Voges J. A randomized trial of deep-brain stimulation for Parkinson's disease. N Engl J Med 2006;355:896–908.

[3] Djaldetti R, Shifrin A, Rogowski Z, Sprecher E, Melamed E, Yarnitsky D. Quantitative measurement of pain sensation in patients with Parkinson disease. Neurology 2004;62:2171–5.

[4] Hagander LG, Midani HA, Kuskowski MA, Parry GJ. Quantitative sensory testing: effect of site and skin temperature on thermal thresholds. Clin Neurophysiol 2000;111:17–22.

[5] Hilker R, Voges J, Weisenbach S, Kalbe E, Burghaus L, Ghaemi M, Lehrke R, Koulousakis A, Herholz K, Sturm V, Heiss WD. Subthalamic nucleus stimulation restores glucose metabolism in associative and limbic cortices and in cerebellum: evidence from a FDG-PET study in advanced Parkinson's disease. J Cereb Blood Flow Metab 2004;24:7–16.

[6] Jaaskelainen SK, Teerijoki-Oksa T, Forssell H. Neurophysiologic and quantitative sensory testing in the diagnosis of trigeminal neuropathy and neuropathic pain. Pain 2005;117:349–57.

[7] Jobst EE, Melnick ME, Byl NN, Dowling GA, Aminoff MJ. Sensory perception in Parkinson disease. Arch Neurol 1997;54:450–4.

[8] Kaji R, Urushihara R, Murase N, Shimazu H, Goto S. Abnormal sensory gating in basal ganglia disorders. J Neurol 2005;252:IV13–6.

[9] Kumar R, Lozano AM, Kim YJ, Hutchison WD, Sime E, Halket E, Lang AE. Double-blind evaluation of subthalamic nucleus deep brain stimulation in advanced Parkinson's disease. Neurology 1998;51:850–65.

[10] Limousin P, Krack P, Pollak P, Benazzouz A, Ardouin C, Hoffmann D, Benabid AL. Electrical stimulation of the subthalamic nucleus in advanced Parkinson's disease. N Engl J Med 1998;339:1105–11.

[11] Lozano AM, Dostrovsky J, Chen R, Ashby P. Deep brain stimulation for Parkinson's disease: disrupting the disruption. Lancet Neurol 2002;1:225–31.

[12] Nolano M, Provitera V, Estraneo A, Selim MM, Caporaso G, Stancanelli A, Saltalamacchia AM, Lanzillo B, Santoro L. Sensory deficit in Parkinson's disease: evidence of a cutaneous denervation. Brain 2008;131:1903–11.

[13] Palmer ST, Martin DJ. Thermal perception thresholds recorded using method of limits change over brief time intervals. Somatosens Mot Res 2005;22:327–34.

[14] Palmer ST, Martin DJ, Steedman WM, Ravey J. Effects of electric stimulation on C and A delta fiber-mediated thermal perception thresholds. Arch Phys Med Rehabil 2004;85:119–28.

[15] Pratorius B, Kimmeskamp S, Milani TL. The sensitivity of the sole of the foot in patients with Morbus Parkinson. Neurosci Lett 2003;346:173–6.

[16] Sandyk R, Snider SR. Sensory symptoms: Parkinson's disease. Neurology 1985;35:619–20.

[17] Schneider JS, Diamond SG, Markham CH. Parkinson's disease: sensory and motor problems in arms and hands. Neurology 1987;37:951–6.

[18] Shy ME, Frohman EM, So YT, Arezzo JC, Cornblath DR, Giuliani MJ, Kincaid JC, Ochoa JL, Parry GJ, Weimer LH. Quantitative sensory testing: report of the therapeutics and technology assessment subcommittee of the American academy of neurology. Neurology 2003;60:898–904.

[19] Taktakishvili O, Sivan-Loukianova E, Kultas-Ilinsky K, Ilinsky IA. Posterior parietal cortex projections to the ventral lateral and some association thalamic nuclei in Macaca mulatta. Brain Res Bull 2002;59:135–50.

[20] Tinazzi M, Recchia S, Simonetto S, Tamburin S, Defazio G, Fiaschi A, Moretto G, Valeriani M. Muscular pain in Parkinson's disease and nociceptive processing assessed with CO_2 laser-evoked potentials. Mov Disord 2010;25:213–20.

[21] Tinazzi M, Del Vesco C, Fincati E, Ottaviani S, Smania N, Moretto G, Fiaschi A, Martino D, Defazio G. Pain and motor complications in Parkinson's disease. J Neurol Neurosurg Psychiatry 2006;77:822–5.

[22] Trost M, Su S, Su P, Yen RF, Tseng HM, Barnes A, Ma Y, Eidelberg D. Network modulation by the subthalamic nucleus in the treatment of Parkinson's disease. Neuroimage 2006;31:301–7.

[23] Verdugo R, Ochoa JL. Quantitative somatosensory thermotest. A key method for functional evaluation of small calibre afferent channels. Brain 1992;115:893–913.

[24] Yarnitsky D. Quantitative sensory testing. Muscle Nerve 1997;20:198–204.

[25] Yarnitsky D, Ochoa JL. Studies of heat pain sensation in man: perception thresholds, rate of stimulus rise and reaction time. Pain 1990;40:85–91.

[26] Zaslansky R, Yarnitsky D. Clinical applications of quantitative sensory testing (QST). J Neurol Sci 1998;153:215–38.

脳神経外科ジャーナル

表題

ブレイン・マシン・インターフェースによる機能支援：リアルタイムロボットアーム制御とワイヤレス完全体内埋込装置の開発

Brain–Machine Interface Using Brain Surface Electrodes: Real-Time Robotic Control and a Fully Implantable Wireless System

著者名

平田雅之[1]、柳澤琢史[1]、松下光次郎[1]、モリスシェイン[1]、神谷之康[2]、鈴木隆文[3]、吉田毅[4]、佐藤文博[5]、齋藤洋一[1]、貴島晴彦[1]、後藤哲[1]、影山悠[1]、川人光男[2]、吉峰俊樹[1]

Masayuki Hirata[1], Takufumi Yanagisawa[1], Kojiro Matsushita[1], Morris Shayne[1], Yukiyasu Kamitani[2], Takafumi Suzuki[3], Tsuyoshi Yoshida[4], Fumihiro Sato[5], Yoichi Saitoh[1], Haruhiko Kishima[1], Tetsu Goto[1], Yu Kageyama[1], Mitsuo Kawato[2], Toshiki Yoshimine[1]

所属

1) 大阪大学大学院医学系研究科脳神経外科学
2) ATR 脳情報研究所
3) 東京大学大学院情報理工学系研究科
4) 広島大学大学院先端物質科学研究科
5) 東北大学大学院医工学研究科

1) Department of Neurosurgery, Osaka University Medical School
2) ATR Brain Information Communication Research Laboratory Group
3) Graduate School of Information Science and Technology, The University of Tokyo
4) Graduate School of Advanced Sciences of Matter, Hiroshima University
5) Group of Electrical Engineering, Communication Engineering, Electronic Engineering, and Information Engineering, Tohoku University

筆頭著者住所(連絡先)

大阪大学大学院医学系研究科脳神経外科学
〒565-0871　大阪府吹田市山田丘 2-2　℡ 06-6879-3652　FAX 06-6879-3659
Email: mhirata@nsurg.med.osaka0u.ac.jp

Department of Neurosurgery, Osaka University Medical School
2-2 Yamadaoka, Suita, Osaka, 565-0871, Japan
Tel:06-6879-3652　Fax:06-6879-3659
Email: mhirata@nsurg.med.osaka0u.ac.jp

図表の数　図　8、表　1 枚

英文抄録(abstract)

Brain–Machine Interface Using Brain Surface Electrodes: Real-Time Robotic Control and a Fully Implantable Wireless System

Masayuki Hirata[1], Takufumi Yanagisawa[1], Kojiro Matsushita[1], Morris Shayne[1], Yukiyasu Kamitani[2], Takafumi Suzuki[3], Tsuyoshi Yoshida[4], Fumihiro Sato[5], Yoichi Saitoh[1], Haruhiko Kishima[1], Tetsu Goto[1], Yu Kageyama[1], Mitsuo Kawato[2], Toshiki Yoshimine[1]

1) Department of Neurosurgery, Osaka University Medical School
2) ATR Brain Information Communication Research Laboratory Group
3) Graduate School of Information Science and Technology, The University of Tokyo
4) Graduate School of Advanced Sciences of Matter, Hiroshima University
5) Group of Electrical Engineering, Communication Engineering, Electronic Engineering, and Information Engineering, Tohoku University

The brain-machine interface (BMI) enables us to control machines and to communicate with others, not with the use of input devices, but through the direct use of brain signals. This paper describes the integrative approach we used to develop a BMI system with brain surface electrodes for real-time robotic arm control in severely disabled people, such as amyotrophic lateral sclerosis patients. This integrative BMI approach includes effective brain signal recording, accurate neural decoding, robust robotic control, a wireless and fully implantable device, and a noninvasive evaluation of surgical indications.

We have previously shown that power in the high gamma band (80 - 150 Hz) gave the highest decoding accuracy. We succeeded in generating voluntary control over the grasping and releasing of objects, using a successive decoding and control algorithm that achieves smooth robotic hand movements. Even in patients with severe motor disturbances, merely imagining hand movements was enough to induce clear, high gamma band responses that were similar to those induced by real movements.

A fully-implantable wireless system is indispensable for the clinical application of invasive BMI in order to reduce the risk of infection. We have developed a prototype which is a 128 channel fully-implantable wireless system that includes many new technologies such as a 64-channel integrated analog amplifier chip, a Bluetooth wireless data transfer circuit, a wirelessly rechargeable battery, 3 dimensional tissue-fitting high density electrodes, a titanium head casing, and a fluorine polymer body casing.

We are planning clinical trials and the introduction of our BMI system after the completion of a two-staged clinical research program using wired and then wireless systems.

Key words
Brain machine interface, Neural decoding, Implant, Functional restoration

要旨

ブレインマシンインターフェース（BMI）は脳信号から運動意図・内容を読み取って外部機器を制御する技術である。我々は脳表電極を用いた BMI により、筋萎縮性側索硬化症等の重症身体障害者に対する機能再建を目指して研究開発を行っている。これまでにγ帯域活動を用いた連続的な解読制御手法により、ロボットアームのリアルタイム制御システムを開発し、脳表電極留置患者による物体の把握･把握解除に成功した。感染リスク回避のためにはワイヤレス体内埋込化が必須であり、ワイヤレス埋込装置のプロトタイプを開発した。

今後は、重症の筋萎縮性側索硬化症を対象として、有線・ワイヤレス埋込の二段階での臨床試験をへて実用化を目指す。

はじめに

Brain-Machine Interface (BMI)とは脳信号を計測してこれをコンピュータで解読(decoding)して、脳信号の意味するところ、すなわち脳機能の内容を推定し、外部機器を操作することにより、失われた神経機能を代行させる技術である(Fig.1)。近年、筋萎縮性側索硬化症(ALS)、脊髄損傷や脳卒中後の運動麻痺をはじめとする脳機能障害患者に対して、BMI 技術を用いて機能補填を図ろうとする研究が盛んになりつつある。

BMI の開発と臨床応用には Table1 にあげるような数多くの要素技術が必要になる。これらは基礎および臨床神経科学 (特に神経生理学や計算機脳科学)、生体医工学、ロボット工学などにかかわる広範な領域にまたがっており、有機的な医工連携、産学連携による統合的な研究開発が必須となる。

こうした状況において、我々は現在、皮質脳波を用いたブレイン・マシン・インターフェースの研究開発を行っており、それは上記のごとく広範囲にわたる。本稿ではその中で特にリアルタイムロボットアーム制御とワイヤレス体内埋込装置について、研究開発の現状を解説する。BMI に関するより一般的な事項についてはすでに別紙で解説しているのでそちらを参照されたい[15]。

Support vector machine を用いた運動内容推定

難治性疼痛に対する運動野電気刺激療法の最適刺激部位同定や、難治性てんかんのてんかん焦点源同定のために硬膜下電極を 2 週間程度留置する場合がある。施設内倫理委員会の承認を得て、これまでにこうした症例約 20 例を対象にして、留置した電極から上肢運動等の課題施行時の皮質脳波を計測し、BMI の研究を行ってきた。

運動企図や運動内容の推定を行う neural decoding(脳信号解読)は BMI の中心となる技術であり、種々の手法が報告されているが、私どもは support vector machine (SVM)という機械学習の手法を中心に用いている。SVM は弁別を行う学習機械のひとつで、弁別空間上に存在する複数個の群を弁別平面で分離する際に互いの距離が最大になるように重み係数を調整することにより高い弁別能を得ようとする手法である[8]。

大脳における運動内容の最終出力部は一次運動野であるが、体性局在があり、ヒトでは一次運動野の大半は中心溝の中に存在すると考えられている．私どもは中心溝内の運動野から直接脳信号を計測すれば、一次運動野の体性局在を最もよく反映した信号を効率よく計測でき、より精密な運動内容推定ができると考えた。

我々の施設では難治性疼痛に対する運動野電気刺激療法において、より効果的疼痛緩和を目的として中心溝内に電極を留置する場合があり、こうした症例 5 例を対象として上肢運動時の皮質脳波計測を行い、SVM を用いて運動内容推定を行った。その結果、中心溝前壁から記録した皮質脳波を用いると、他の部位よりも有意に高い正解率で運動内容推定ができることが明らかになった[10]。

部位とともに、どのような神経生理学的特徴量が運動内容推定に有用かを明らかにすることも重要である。最近、高周波帯域に運動情報が豊富に含まれているとの報告が増えている[2]。そこで我々は皮質脳波のどの周波数帯域が運動内容推定に有用であるかを調べた。その結果、γ帯域(80－150Hz)のパワーが運動内容推定に有用であることを明らかにした[9]。さらに被験者の運動障害の有無によらず、γ帯域のパワーを用いると高い運動内容推

定の正解率が得られることが明らかになった(Fig.2)[11]。運動障害の強い症例ではγ帯域活動の強度は運動障害の強い症例より減弱しているものの、運動想起だけで明瞭なγ帯域活動が生じ、これを用いて運動内容推定が可能であることを明らかにした。

ロボットアームのリアルタイム制御

次いで、こうした運動内容推定技術を応用して義手ロボットをリアルタイムに制御するシステムを開発した(Fig.3)[11]。このシステムを用いて、難治性てんかんや難治性疼痛の治療目的で硬膜下電極を留置された患者さんの協力を得て、皮質脳波による義手ロボットのリアルタイムコントロールの実証研究を行っている。

まず、手の把握、つまむ、開くや肘の屈曲といった基本的な上肢の運動要素を各 40 回程度行い、これを SVM の学習データとしてパラメータ設定をおこない、次にそのパラメータ設定を用いてリアルタイムに連続的な decoding と制御を行う。最近では Gaussian process regression という手法を用いて運動推定がどの程度正確にできるかを評価し、運動推定が正確にできると評価された時に限り、SVM による decoding を行うことにより、外乱ノイズに強いロバストな制御ができるようにしている(Fig.3)[11]。これらの結果、運動 1 回毎の皮質脳波による運動の推定精度は 60~80%とリアルタイム制御に利用しうる推定精度が得られた。この推定精度は完全とは言えないが、ロバストな運動推定・ロボット制御法を導入することにより、手から肘までの制御や、物の把握や把握解除など実用的な動作ができつつある(Fig.4)[11]。また、硬膜下電極を用いた皮質脳波計測は長期間安定していることが動物実験で明らかになっている。我々の臨床例でも約 2 週間という短期間の電極留置ではあるが、初回の実験から 4 日後でも初回の設定パラメータを利用して、リアルタイムロボットアーム制御により、物体の把握・把握解除ができることを示せた[11]。

ワイヤレス体内埋込装置の開発

臨床応用に際しては感染リスク低減のためにワイヤレス完全埋込化が必須であるが、刺激型の体内埋込装置とことなり、BMI の臨床用ワイヤレス埋込装置はこれまでほとんど報告がない。唯一 kennedy らのグループが電極数わずか 2ch の装置を報告しているのみである[3]。

そこで現在我々は電極数 100ch 以上の臨床用ワイヤレス埋込 BMI 装置の実用化を目指して現在開発を行っており、プロトタイプを試作した。Fig.5A に今回開発したワイヤレス完全埋込装置のシステム構成を示す。Fig.5B に今回開発したプロトタイプを示す。本装置は頭部装置と腹部装置からなる。頭部装置は、3 次元高密度両面電極、マルチチャンネル集積化アンプとアンプを収納する人工頭蓋骨兼用頭部ケーシングからなる。腹部装置は、ワイヤレスデータ通信回路、非接触充電電源とそれらを収納するフッ素ポリマー樹脂からなる。

3 次元高密度両面電極

皮質脳波計測用のグリッド電極はテーラーメイドにより個々人の脳形状にフィットするものを考案した[6; 17]。脳表面形状抽出は、Thin slice MRI 画像を用いて行い、特に脳溝形状データについては自動脳溝抽出ソフト(Brain VISA, http://brainvisa.info/)を用いた形

状抽出を行う。これらの脳形状データから3次元CAD(3 matic, Materialize Japan, Tokyo)上で電極配置を最適化してシート型の設計を行い、3 次元プリンタで型を迅速製造する。個々人の脳形状に密着するため、全ての電極から精度の高い皮質脳波が計測でき、脳への圧迫も少ない。電極間距離は最短 2.5mm で従来の電極間隔 10mm に比較して 16 倍高密度化した。電極は電極径 1mm の白金電極を用いている。極端に小型化すると計測安定性が低下する懸念があるが、同一の電極を用いたサルの実験で1年間にわたり安定して計測できることが示されている[1)]。脳溝内に挿入する場合には両面に電極を配置できる(Fig.6)。脳溝内の大脳皮質の両面から皮質脳波を計測することにより、より広範囲からの脳信号計測が可能となる。また、本電極により大脳皮質を電気刺激することも可能であり、特に中心溝に挿入した場合には体性感覚野側は電気刺激による感覚フィードバックに応用することも可能である。

マルチチャンネル集積化アンプ

計測した皮質脳波はノイズ混入を防ぐため、すぐに増幅・デジタル化する必要がある。そこで頭部の狭小なスペースに留置できるよう皮質脳波を増幅するアナログアンプを集積化した。1 チップあたり 64ch を有し、各 ch は 1kHz でのサンプリングが可能であり、AD コンバーターは 12bit、チップサイズは 5×5mm、消費電力は 4.9mW である[12; 13)]。東京大学 VDEC の CMOS 0.18 um プロセスにて製造した。これを 2 チップ計 128ch として 30×20×2.5mm 大の小型基板上に実装する(Fig.7)。この集積化アンプ実装基板は人工骨兼用頭部ケーシングに収納される。

人工頭蓋骨兼用頭部ケーシング

頭部ケーシングは、集積化アンプを収容し、開頭部の人工頭蓋骨を兼ねるものを考案した[5; 16)]。Thin slice bone window CT 画像から 3 次元 CAD(3 matic, Materialize Japan, Tokyo)上で、開頭範囲、人工頭蓋骨の形状、電子回路のレイアウト設計を行い、3 次元 CAM (Gibbs CAM, Gibbs and Associates, USA)で切削パスを作成し、迅速製造する(Fig.8)。患者 CT 画像から骨データを抽出して作成し、人工頭蓋骨を兼ねるため埋込による皮膚膨隆がなく、整容学的に優れ、瘻孔形成等のリスクも低い。開頭は頭部ケーシングに合わせて正確に開頭する必要があるため、頭部ケーシングの位置形状データをナビゲーションにあらかじめレジストレーションしておき、ナビゲーションガイド下に開頭を行う。

ワイヤレスデータ通信

体外への皮質脳波の伝送には、Bluetooth プロトコル(Class2)を用いたワイヤレスデジタル通信を採用し、信頼性を確保している。Bluetooth 回路を 2 ヶ使用することにより 400kbps のデータ通信速度を確保し、皮質脳波を 12bit×128ch で体外のコンピュータに送信する。しかし、現状では消費電力は 300mW と大きく、埋込装置の消費電力の大半を占める。サイズも現状では 60×60×8mm と大きい。今後さらに高速化、小型化、低電力化が必要であり、その解決方法として、ワイヤレス LAN や UWB といった通信プロトコルの導入が考えられる。

非接触充電電源

必要な電力を確保するため本システムでは非接触給電機能を持たせた。体外の送電回路と体内の受電回路からなる。コイル誘導起電方式により、直径 40mm のコイルを用いて、皮下 4cm で 4W と大きな給電能力を持つ。

フッ素ポリマー樹脂腹部ケーシング

ワイヤレス通信回路と非接触充電電源はシリコーンで包埋し、さらにこれをフッ素ポリマー樹脂でパッケージングし、腹部装置を構成する。腹部装置は腹部皮下に留置する。フッ素ポリマー樹脂ケーシングは耐腐食性、生体適合性が高いだけでなく、従来のチタンケーシングに比較してコスト低減も期待できる。

知財戦略とインフラ整備

知財戦略は企業が市場化を行う際に重要であるだけでなく、自らの開発戦略を守りスムーズに進め、さらには日本の科学技術戦略のためにも重要である。そこで我々は開発における発明要素を可能な限り特許出願・取得に結び付けるよう努力しており、これまでに BMI 関係の特許出願を国内・国際合わせて 6 件行い[4; 5; 7; 16-18]、うち 1 件を特許取得した[6]。

また一般的に埋込医療機器開発は欧米に対して大きく遅れており、本邦の研究機関・企業・審査機関は埋込医療機器の臨床応用・実用化に関する経験に乏しい。こうした状況を少しでも改善すべく、厚生労働省の次世代医療機器評価指標作成事業にて神経機能修復装置に関する評価指標を作成した[14]。こうしたガイドラインの整備は、企業の開発目標レベルの設定の明確化や将来の薬事承認審査の迅速化につながるものと期待される。

今後の展望

現在、ワイヤレス埋込装置プロトタイプを動物埋込用に改造して動物実験を開始したところである。今後、ALS 患者等の重症身体障害者を対象として、有線・ワイヤレス埋込の二段階での臨床研究を経て、治験・実用化を目指す。

謝辞

本研究は文部科学省の脳科学研究戦略推進プログラム「日本の特長を活かしたＢＭＩの統合的研究開発」、ならびに厚生労働省の厚生労働科学研究費補助金 医療技術実用化総合研究事業により行われている。

文献

1) Chao ZC, Nagasaka Y,Fujii N: Long-term asynchronous decoding of arm motion using electrocorticographic signals in monkeys. *Front Neuroengineering* **3**:3, 2010.

2) Crone NE, Sinai A,Korzeniewska A: High-frequency gamma oscillations and human brain mapping with electrocorticography. *Prog Brain Res* **159**:275-295, 2006.

3) Guenther FH, Brumberg JS, Wright EJ, Nieto-Castanon A, Tourville JA, Panko M,

Law R, Siebert SA, Bartels JL, Andreasen DS, Ehirim P, Mao H,Kennedy PR: A wireless brain-machine interface for real-time speech synthesis. *PLoS One* **4**:e8218, 2009.

4) Hirata M, Yanagisawa T, Kamitani Y, Yokoi H, Yoshimine T, Goto T, Fukuma R,Kato R: Machine control device, machine system, machine control method, and recording medium storing machine control program. US patent application, 12/799,840, 2010.

5) Hirata M, Yoshimine T, Matsushita K, Goto T, Yanagisawa T, Suzuki T,Yoshimoto S: PCT patent application, PCT/JP2011/001402, 2011.

6) Hirata M, Yoshimine T, Saitoh Y, Yanagisawa T, Goto T, Watanabe Y,Saito T: Intracranial electrode and method for producing same. US patent, US7,860,577, 2010.

7) Hirata M, Yoshimine T, Saitoh Y, Yanagisawa T, Goto T, Watanabe Y,Saito T: Intracranial electrode and method for producing same. US patent application, 12/378,695, 2009.

8) Kamitani Y,Tong F: Decoding the visual and subjective contents of the human brain. *Nat Neurosci* **8**:679-685, 2005.

9) Yanagisawa T, Hirata M, Saitoh Y, Goto T, Kishima H, Fukuma R, Yokoi H, Kamitani Y,Yoshimine T: Real-time control of a prosthetic hand using human electrocorticography signals. *J Neurosurg* **114**:1715-1722, 2011.

10) Yanagisawa T, Hirata M, Saitoh Y, Kato A, Shibuya D, Kamitani Y,Yoshimine T: Neural decoding using gyral and intrasulcal electrocorticograms. *Neuroimage* **45**:1099-1106, 2009.

11) Yanagisawa T, Hirata M, Saitoh Y, Kishima H, Matsushita K, Goto T, Yokoi H, Kamitani Y,Yoshimine T: Electrocorticographic control of a prosthetic arm in paralyzed patients. *Ann Neurol*, in press.

12) Yoshida T, Masui Y, Eki R, Iwata A, M. Y,Uematsu K: A Neural Recording Amplifier with Low-Frequency Noise Suppression. *IEICE Trans Electrons* **E93-C**:849-854, 2010.

13) Yoshida T, Sueishi K, Iwata A, Matsushita K, Hirata M,Suzuki T: A High-Linearity Low-Noise Amplifier with Variable Bandwidth for Neural Recording Systems. *Japanese Journal of Applied Physics* **50**, 2011.

14) 厚生労働省医薬食品局・医療機器審査管理室: 次世代医療機器評価指標の公表について（平成 22 年 12 月 15 日薬食機発 1215 第 1 号）. 2010.

15) 平田雅之,吉峰俊樹: 脳神経外科における BMI の展望. *脳神経外科速報* **21**:880-889, 2011.

16) 平田雅之, 吉峰俊樹, 松下光次郎, 後藤哲, 柳澤琢史, 鈴木隆文,吉村眞一: 体内埋込装置のケーシングと体内埋込装置、および体内埋込装置のケーシングの製造方法. 日本, 特願 2010 - 250464, 2010.

17) 平田雅之, 吉峰俊樹, 齋藤洋一, 柳澤琢史,後藤哲: 頭蓋内電極構造体およびその製造方

法. 日本, 特願 2007-216461, 2007.
18) 平田雅之, 柳澤琢史, 神谷之康, 横井浩史, 吉峰俊樹, 後藤哲, 福間良平,加藤龍: 機器制御装置、機器システム、機器制御方法、機器制御プログラム、および記録媒体. 日本, 特願 2010 - 49814, 2010.

Figure Legend

Fig.1 A conceptual diagram of brain machine interface

Fig.2 Time-frequency distribution of decoding accuracy in subjects with no motor dysfunction, moderate motor dysfunction and severe motor dysfunction.

Fig. 3 A real-time BMI system for robotic arm control.

Fig.4 Real-time control of a robotic arm. The subject voluntarily controlled grasping (upper right) and hand-opening (upper left) of the robotic arm in real time. The hand and elbow of the robotic arm were controlled simultaneously and independently (lower right and left).

Fig.5 Schematic diagram of the fully-implantable wireless system. (A) and the first prototype of the fully-implantable wireless system (B, C)
a: Fluorine polymer body casing including a wireless rechargeable unit and a wireless data transfer unit. b: A titanium head casing / artificial skull bone. c: Brain surface microelectrodes conformable to the outer surface of the individual brain. d: Brain surface microelectrodes conformable to the central sulcus.

Fig. 6 Three dimensional high density grid electrodes
A: high density electrodes (upper) and standard electrodes (lower), B: brain surface electrodes conformable to individual brain surface, C: intrasulcal electrodes, D: automatic sulcal detection and mold design on 3D CAD.

Fig. 7 Integrated analog amplifier.
A: Target frequency bands and gains to cover electrocorticographic signals and local field potentials (LFP). B: A 64-channel integrated analog amplifier chip (5 x 5 mm). C: A 128-channel integrated analog amplifier board (30 x 20 mm)

Fig.8 A titanium head casing / artificial skull bone.
A: Simulation of machining process. B, C: Head casing designed using 3D CAD software. Three dimensional skull bone data were obtained from individual's CT

images. B: A head casing attached to the skull. C: Inner side view. The head casing contains 128-channel integrated amplifier board on a small mounting board which is mounted on a folded inner panel as indicated in a green color. D: A prototype casing. Upper: inner side view. Lower: outer side view. E: A prototype head casing attached to the skull model.